THE ASTROPHYSICAL JOURNAL, 432:158–166, 1994 September 1

EXCITATION OF INTERSTELLAR HYDROGEN CHLORIDE

DAVID A. NEUFELD
Johns Hopkins University, Department of Physics and Astronomy, 3400 North Charles Street, Baltimore, MD 21218
AND
SHELDON GREEN
NASA/Goddard Space Flight Center, Institute for Space Studies, 2880 Broadway, New York, NY 10025
Received 1993 October 25; accepted 1994 February 25

ABSTRACT

We have computed new rate coefficients for the collisional excitation of HCl by He, in the close-coupled formalism and using an interaction potential determined recently by Willey, Choong, & DeLucia. Results have been obtained for temperatures between 10 K and 300 K. With the use of the infinite order sudden approximation, we have derived approximate expressions of general applicability which may be used to estimate how the rate constant for a transition $(J \rightarrow J')$ is apportioned among the various hyperfine states F' of the final state J'. Using these new rate coefficients, we have obtained predictions for the HCl rotational line strengths expected from a dense clump of interstellar gas, as a function of the HCl fractional abundance. Over a wide range of HCl abundances, we have found that the line luminosities are proportional to (abundance)$^{2/3}$, a general result which can be explained using a simple analytical approximation. Our model for the excitation of HCl within a dense molecular cloud core indicates that the $J = 1$–0 line strengths measured by Blake, Keene, & Phillips toward the Orion Molecular Cloud (OMC-1) imply a fractional abundance $n(\mathrm{HCl})/n(\mathrm{H_2}) \sim 2 \times 10^{-9}$, a value which amounts to only $\sim 0.3\%$ of the cosmic abundance of chlorine nuclei. Given a fractional abundance of 2×10^{-9}, the contribution of HCl emission to the total radiative cooling of a dense clump is small. For Orion, we predict a flux $\sim 10^{-19}$ W cm^{-2} for the HCl $J = 3$–2 line near 159.8 μm, suggesting that the strength of this line could be measured using the *Infrared Space Observatory*.

Subject headings: ISM: molecules — molecular data — molecular processes — radio lines: ISM

1. INTRODUCTION

Because of their large rotational constants and spontaneous radiative rates, simple hydrides are potentially important coolants of dense interstellar gas (Goldsmith & Langer 1978). Theoretical studies (e.g., Neufeld, Lepp, & Melnick 1994) have shown water to be the major coolant of dense molecular cloud cores, although space-based observations are still needed to confirm the molecular abundances predicted in these studies and upon which the water cooling rate is premised. Hydrogen chloride would also be a significant coolant in dense regions (Dalgarno et al. 1974; Goldsmith & Langer 1978) were its abundance $x(\mathrm{HCl}) \equiv n(\mathrm{HCl})/n(\mathrm{H_2})$ as large as $\sim 10^{-7}$. Fortunately, observations of interstellar HCl are possible from suborbital observatories and have been carried out by Blake, Keene, & Phillips (1985, hereafter BKP), who used the Kuiper Airborne Observatory to detect emission in the $J = 1$–0 line of $\mathrm{H^{35}Cl}$ near 625.9 GHz toward OMC-1. These observations were interpreted as indicating an HCl abundance of $x(\mathrm{HCl}) = 5$–50×10^{-9}.

In the study presented here, we have reinterpreted the BKP observations using newly computed rate coefficients for the collisional excitation of HCl by He. Our computation of the rate coefficients is described in § 2. Using these new molecular data, we have modeled the excitation of HCl within the Orion region, with full account taken of optical depth effects, as described in § 3. Our results are discussed in § 4 and a brief summary is given in § 5.

2. RATE COEFFICIENTS FOR COLLISIONAL EXCITATION OF HCl

Earlier theoretical studies of rotational excitation of HCl by collisions with He determined the interaction forces from approximate theoretical methods based on either an electron gas model (Green & Monchick 1975) or an electron-atom pseudopotential model (Collins & Lane 1975). Estimates of the spherical average of the potential have been obtained experimentally from analysis of molecular beam scattering data (Held et al. 1980) and from infrared spectra of the van der Waals complex (Lovejoy & Nesbitt 1990). Willey, Choong, & DeLucia (1992), who recently measured pressure-broadened widths of the lowest rotational line of DCl in He at cryogenic temperatures, noted that the earlier interaction potentials are not in particularly good agreement with each other and that neither the electron gas nor the electron-atom pseudopotential interactions are able to predict their measured line widths. However, predictions from the latter potential were closer to experimental values, and they were able to find a modification of this potential which did provide agreement with their low-temperature line width parameters and also with room temperature values. They noted that the spherical average of the resulting potential is in harmony with the beam scattering and van der Waals dimer results. Pressure-broadened line widths are sensitive to anisotropies in the interaction potential and provide an approximate measure of total excitation rates out of the spectral levels, so this potential should provide reasonably accurate values for rotational excitation rates.

The interaction potential obtained by Willey et al. (1992) is used here to calculate state-to-state collisional excitation rates of HCl by He. For molecular scattering calculations the interaction potential must be measured from the center of mass of the rotor. The analytic form given for DCl–He by Willey et al. (1992) was transformed numerically to HCl coordinates (using $\mathrm{H^{35}Cl}$) and expanded in Legendre polynomials via 11-point Gauss quadrature, retaining terms through P_5, one higher than

TABLE 1

RATE COEFFICIENTS FOR COLLISIONAL EXCITATION OF HCl BY He (cm^3 s^{-1})

	TEMPERATURE							
J_i–J_f	10 K	20 K	30 K	50 K	80 K	100 K	200 K	300 K
1–0	3.35 (−12)[a]	4.20 (−12)	5.09 (−12)	6.88 (−12)	9.29 (−12)	1.07 (−11)	1.54 (−11)	1.80 (−11)
2–0	9.12 (−13)	1.02 (−12)	1.20 (−12)	1.73 (−12)	2.83 (−12)	3.67 (−12)	8.15 (−12)	1.22 (−11)
2–1	1.77 (−11)	1.86 (−11)	1.93 (−11)	2.10 (−11)	2.36 (−11)	2.52 (−11)	3.11 (−11)	3.44 (−11)
3–0	1.92 (−12)	2.09 (−12)	2.24 (−12)	2.54 (−12)	2.91 (−12)	3.10 (−12)	3.67 (−12)	3.98 (−12)
3–1	3.52 (−12)	3.83 (−12)	4.18 (−12)	5.08 (−12)	6.82 (−12)	8.12 (−12)	1.49 (−11)	2.08 (−11)
3–2	1.97 (−11)	2.08 (−11)	2.16 (−11)	2.36 (−11)	2.67 (−11)	2.87 (−11)	3.69 (−11)	4.27 (−11)
4–0	8.83 (−13)	8.04 (−13)	8.38 (−13)	1.01 (−12)	1.32 (−12)	1.54 (−12)	2.52 (−12)	3.25 (−12)
4–1	1.58 (−12)	1.43 (−12)	1.49 (−12)	1.81 (−12)	2.39 (−12)	2.79 (−12)	4.81 (−12)	6.69 (−12)
4–2	4.99 (−12)	4.43 (−12)	4.52 (−12)	5.30 (−12)	6.94 (−12)	8.17 (−12)	1.47 (−11)	2.08 (−11)
4–3	2.98 (−11)	2.53 (−11)	2.45 (−11)	2.61 (−11)	2.95 (−11)	3.18 (−11)	4.06 (−11)	4.65 (−11)
5–0	1.63 (−13)	1.60 (−13)	1.78 (−13)	2.49 (−13)	3.96 (−13)	5.12 (−13)	1.20 (−12)	1.90 (−12)
5–1	6.64 (−13)	6.45 (−13)	6.96 (−13)	9.17 (−13)	1.32 (−12)	1.60 (−12)	3.01 (−12)	4.30 (−12)
5–2	7.36 (−13)	7.12 (−13)	7.66 (−13)	9.98 (−13)	1.42 (−12)	1.72 (−12)	3.26 (−12)	4.76 (−12)
5–3	3.98 (−12)	3.79 (−12)	3.97 (−12)	4.94 (−12)	6.76 (−12)	8.04 (−12)	1.46 (−11)	2.06 (−11)
5–4	2.32 (−11)	2.14 (−11)	2.14 (−11)	2.43 (−11)	2.92 (−11)	3.22 (−11)	4.33 (−11)	5.03 (−11)
6–0	4.68 (−15)	1.18 (−14)	1.70 (−14)	2.85 (−14)	5.19 (−14)	7.27 (−14)	2.35 (−13)	4.39 (−13)
6–1	4.62 (−14)	1.16 (−13)	1.64 (−13)	2.66 (−13)	4.50 (−13)	5.92 (−13)	1.42 (−12)	2.26 (−12)
6–2	1.23 (−13)	3.04 (−13)	4.25 (−13)	6.62 (−13)	1.05 (−12)	1.32 (−12)	2.69 (−12)	3.95 (−12)
6–3	1.42 (−13)	3.48 (−13)	4.81 (−13)	7.26 (−13)	1.11 (−12)	1.37 (−12)	2.75 (−12)	4.09 (−12)
6–4	8.72 (−13)	2.13 (−12)	2.88 (−12)	4.22 (−12)	6.19 (−12)	7.51 (−12)	1.39 (−11)	1.96 (−11)
6–5	4.89 (−12)	1.17 (−11)	1.53 (−11)	2.07 (−11)	2.72 (−11)	3.09 (−11)	4.42 (−11)	5.26 (−11)
7–0	3.62 (−15)	6.65 (−15)	8.94 (−15)	1.39 (−14)	2.40 (−14)	3.25 (−14)	8.61 (−14)	1.39 (−13)
7–1	1.51 (−14)	2.76 (−14)	3.71 (−14)	5.79 (−14)	1.03 (−13)	1.43 (−13)	4.11 (−13)	6.82 (−13)
7–2	5.85 (−14)	1.07 (−13)	1.42 (−13)	2.16 (−13)	3.60 (−13)	4.79 (−13)	1.19 (−12)	1.85 (−12)
7–3	1.35 (−13)	2.44 (−13)	3.20 (−13)	4.71 (−13)	7.40 (−13)	9.45 (−13)	2.05 (−12)	3.02 (−12)
7–4	2.13 (−13)	3.79 (−13)	4.90 (−13)	6.95 (−13)	1.04 (−12)	1.30 (−12)	2.67 (−12)	3.87 (−12)
7–5	1.25 (−12)	2.20 (−12)	2.81 (−12)	3.86 (−12)	5.57 (−12)	6.80 (−12)	1.29 (−11)	1.80 (−11)
7–6	7.29 (−12)	1.25 (−11)	1.54 (−11)	1.96 (−11)	2.53 (−11)	2.88 (−11)	4.34 (−11)	5.34 (−11)

[a] $X(-Y)$ means $X \times 10^{-Y}$.

retained for the DCl–He interaction. Resulting Legendre radial coefficients were tabulated for collision distances between 1.0 and 10.9 Å in steps of 0.1 Å, and continuous radial functions needed for the molecular scattering calculations were obtained by fifth-order polynomial interpolation (Green 1977a).

Collision cross sections were obtained within the essentially exact close-coupling formalism, retaining at least two energetically closed rotational levels to ensure convergence. Calculations were done with the MOLSCAT[1] computer code using the hybrid modified log-derivative-Airy propagator of Alexander & Manolopoulos (1987) to integrate the radial equations and choosing numerical tolerances to provide accuracy of generally better than three significant figures. Errors from numerical solution of the molecular scattering equations are thus negligible compared with errors due to probable remaining inaccuracies in the interaction potential. To obtain thermal averages, cross sections were calculated for over a hundred energies using a closely spaced grid near thresholds to ensure accuracy at low temperatures and extending to a total energy of over 1800 K. For total energies above 1200 K the computationally cheaper coupled states approximation was used. This approximation was compared with close coupling at an energy of 900 K and found to be accurate to generally better than 10%; it is expected to become more accurate at higher collision energies. Since values in the high-energy tail of the Boltzmann distribution contribute only slightly to thermal averages at the temperatures of interest, this is a negligible source of error. Resulting rate constants are given in Table 1 for temperatures between 10 and 300 K.[2]

Pressure-broadening cross sections were also calculated, and these are compared with experimental values (Giraud, Robert, & Galatry 1979) in Table 2. Theory predicts values essentially independent of rotational level while the experimental results indicate that the 0–1 line is some 30% wider than higher rotational lines. Considering typical uncertainties in early line width measurements and the simplicity of the theoretical interaction potential used here, this agreement is rather good.

Resulting state-to-state excitation rates calculated here are not too different from values obtained previously with the

TABLE 2

THEORETICAL AND EXPERIMENTAL ROOM TEMPERATURE LINE WIDTH CROSS SECTIONS (Å^2)

J–J'	Theory	Experimental[a]
0–1	9.8	13.2
1–2	9.4	
2–3	9.5	
3–4	...	8.6

[a] Giraud, Robert, & Galatry 1970.

[1] J. M. Hutson and S. Green, MOLSCAT computer code, version 12 (1993), distributed by Collaborative Computational Project No. 6 of the Science and Engineering Research Council, UK. Further information can be obtained from J. M. Hutson, Department of Chemistry, University of Durham, Science Laboratories, South Road, Durham DH1 3LE, UK.

[2] Computer files containing this data set and specifying the apportionment of these rate constants among the various hyperfine states of the final rotational state may be obtained from S. Green. Requests may be sent electronically via the Bitnet network to AGXSG@NASAGISS or via Internet to agxsg@nasagiss.giss.nasa.gov.

electron-gas potential (S. Green, unpublished). The dominant $\Delta J = 1$ rates generally agree within 20%–30% with earlier values. The current results for $\Delta J > 1$ rates, however, decrease faster with ΔJ than did the earlier values.

In the interstellar gas H_2 molecules are the dominant collision partner, being some 5 times more abundant than He atoms. However, calculations for excitation of HCl by H_2 are significantly more difficult for two reasons. First, the interaction potential depends on an additional angular degree of freedom; an accurate HCl–H_2 interaction potential is not currently available. Second, H_2 rotational basis functions greatly increase the number of coupled channels in the scattering calculation. To some extent excitation by He and by H_2 are expected to be similar and it may be possible to make reasonable estimates for the latter from the former. Major differences are expected to come from the smaller mass and hence higher velocity of H_2, which leads to larger rate constants even if the collision cross sections are the same, and from the long-range interaction between the HCl dipole moment and the H_2 quadrupole moment. Because of the first factor, to a first approximation, excitation rates for H_2 are about 40% larger than those for He collisions. The second factor is more complex because the long-range dipole-quadrupole interaction is quenched if H_2 is constrained to its lowest, $J = 0$, rotational level, as may be the case at low interstellar temperatures if the ortho-para ratio is thermalized. If the H_2 molecules are in higher rotational levels the long-range interaction is expected to enhance dipole allowed transitions in HCl, i.e., those which change the HCl rotational level by $\Delta J = \pm 1$. Model calculations for HCl–H_2 (Green 1977b) support this expectation, and indicate an enhancement in these rates by a factor of 2–3 with little change in rates for $|\Delta J| > 1$. Thus, to model excitation by interstellar H_2, the rates calculated here should be multiplied by a factor of 1.4; to the extent that H_2 is expected to be in excited rotational states, the rates for $\Delta J = \pm 1$ transitions should be further increased by a factor of 2.5.

Because nuclear hyperfine structure (HFS) is resolved in some of the astrophysical spectra it is desirable to obtain rates among these levels which are labeled by J and F, where J is the usual rotational quantum number and F, the total angular momentum, is obtained by coupling J to I, the nuclear spin; $I = 3/2$ for both ^{35}Cl and ^{37}Cl. The nuclear spin is coupled only weakly to molecular motion and, to an excellent approximation, does not affect collision dynamics. In that case it is straightforward to transform collisional S-matrices determined in the usual manner (i.e., ignoring nuclear spin) into an appropriately recoupled basis set, and these can be used to calculate rates among the HFS levels (Corey & McCourt 1983; Monteiro & Stutzki 1986; Green 1988). Although straightforward, the angular momentum recoupling is computationally intensive. Further, it is difficult within this framework to make modifications that might account for the difference between H_2 and He as collision partners.

Another approach takes advantage of simplifications that arise in the infinite order sudden (IOS) approximation to collision dynamics in which rotational energy spacings are ignored compared with the collision energy. In this approximation the entire matrix of state-to-state rate constants can be calculated in terms of the rates out of the lowest, $J = 0$, level:

$$\gamma^{\rm IOS}(J \to J') = [J'] \sum_L \begin{pmatrix} J & J' & L \\ 0 & 0 & 0 \end{pmatrix}^2 \gamma^{\rm IOS}(0 \to L) , \quad (2.1)$$

where $[a, b, \ldots] = (2a + 1)(2b + 1) \ldots$ and

$$\begin{pmatrix} J & J' & L \\ 0 & 0 & 0 \end{pmatrix}$$

is a 3-j vector coupling coefficient. The rates among HFS levels can be similarly calculated (Corey & McCourt 1983; Varshalovich & Khersonsky 1977 obtained essentially the same formula from a different approach):

$$\gamma^{\rm IOS}(JF \to J'F') = [J, J', F'] \times \sum_L \begin{pmatrix} J & J' & L \\ 0 & 0 & 0 \end{pmatrix}^2 \begin{Bmatrix} L & F & F' \\ I & J' & J \end{Bmatrix}^2 \gamma^{\rm IOS}(0 \to L) , \quad (2.2)$$

where

$$\begin{Bmatrix} L & F & F' \\ I & J' & J \end{Bmatrix}$$

is a 6-j angular momentum recoupling coefficient. Unfortunately, the rotational energy spacings in HCl are not particularly small compared to the collision energies of interest here, and the IOS approximation for the matrix of state-to-state rates is only moderately accurate. However, the HFS splittings are negligible compared with the collision energies, and it is expected that the IOS prescription is accurate for predicting relative rates among different HFS levels within a $(J \to J')$ transition. Thus, one would scale the close coupling $\gamma(J \to J')$ as

$$\gamma(JF \to J'F') = \frac{\gamma^{\rm IOS}(JF \to J'F')}{\gamma^{\rm IOS}(J \to J')} \gamma(J \to J') , \quad (2.3)$$

using the actual (close coupling) rates for the IOS "fundamental" rates, $\gamma^{\rm IOS}(0 \to L)$. Rates among HFS levels within the same rotational state, J, require special consideration. Direct application of the above scaling would use the elastic rates, $\gamma(J \to J)$, which are generally several orders of magnitude larger than the inelatic rates. In fact, it can be shown that these elastic rates contribute only to the elastic HFS rates, $\gamma(JF \to JF)$, and these are not of interest as they do not transfer population. For $\gamma(JF \to JF')$, with $F \neq F'$, one can use the formula for $\gamma^{\rm IOS}(JF \to JF')$ directly, i.e., without scaling to close coupling rates, but using close coupling values for the fundamental $\gamma(0 \to \rm L)$ rates.

An even simpler approximation can be obtained by noting that the fundamental rates generally decrease rapidly with L. If only the largest term, which corresponds to $L = |J - J'|$, is retained in $\gamma^{\rm IOS}(JF \to J'F')$ and $\gamma^{\rm IOS}(J \to J')$, one obtains the simple scaling relationship

$$\gamma(JF \to J'F') = [J, F'] \begin{Bmatrix} |J - J'| & F & F' \\ I & J' & J \end{Bmatrix}^2 \gamma(J \to J') . \quad (2.4)$$

It is readily shown for both this and the full IOS scaling that

$$\sum_{F'} \gamma(JF \to J'F') = \gamma(J \to J') , \quad (2.5)$$

as required. Although the simpler scaling relationship was found to be accurate to better than 20% compared with the full IOS scaling, the latter was used to obtain rates among HFS levels in the present work.

This IOS scaling method should be generally useful for obtaining rates among HFS levels for other systems for which

state-to-state rotational excitation rates are known. In this context, note that it provides a rather good description of the accurate close coupling HFS excitation rates calculated by Monteiro & Stutzki (1986) for HCN at quite low kinetic temperatures, 10–30 K.

3. HCl LINE STRENGTHS

Like other diatomic hydrides, HCl possesses a large rotational constant in comparison to nonhydrides ($B = 10.4$ cm^{-1}), and consequently a large spontaneous radiative rate for the $J = 1$–0 rotational transition ($A_{10} = 1.2 \times 10^{-3}$ s^{-1}). This leads to a large value for the critical density, n_{cr}, at which the spontaneous radiative rate equals the rate of collisional deexcitation. At a temperature of 100 K, the results presented in Table 1 imply that $n_{cr} = 4 \times 10^7$ cm^{-3} for the $J = 1$–0 transition. This value for n_{cr} implies that the emission from interstellar HCl tends to originate primarily in dense cloud cores.

We have derived HCl line strengths for dense cloud cores, treating them as singular isothermal spheres with an assumed density profile of the form $n(H_2) = \kappa r^{-2}$, where r is the distance from the center of the core and κ is a constant. Our choice of this model is motivated both by observational considerations (e.g., Goldsmith et al. 1980; Keto, Ho, & Haschick 1988; Myers & Fuller 1992; Fuller & Myers 1993) and by the fact that theoretical models of star formation (e.g., Larson 1969) predict evolution toward a $1/r^2$ density dependence in star-forming cloud cores even if the initial state of the gas is homogeneous. In this paper we assume that any bulk fluid motions in the cloud core are small compared to the line width, as the observations of Goodman et al. (1993) have suggested to be the case in most cloud cores. However, as described in Appendix B, the results obtained here may be straightforwardly rescaled so as to apply to the case of a constant velocity outflow, in which a $1/r^2$ density dependence would also obtain.

At any point in the cloud core, the emission rate per HCl molecule in any given line is a function of three variables: the H_2 density, $n(H_2)$, the gas temperature T, and an optical depth parameter, $\tilde{N}$(HCl), which has been defined by Neufeld & Kaufman (1993, hereafter NK93). In the geometry considered here, $\tilde{N}(\mathrm{HCl}) \sim N(\mathrm{HCl})/\Delta v(\mathrm{HCl})$, where N(HCl) is the column density measured along a radial path from any point in the core out to the surface, and Δv(HCl) is the Doppler width of the HCl line profile (i.e., the "Doppler parameter," sometimes denoted "b," which is a factor $2^{1/2}$ larger than the one-dimensional velocity dispersion of the HCl molecules). Note that Δv(HCl) is related to the underlying velocity dispersion: the actual observed line may be broadened by optical depth effects. For the singular isothermal sphere, the constant of proportionality κ is given by

$$\kappa = \frac{\Delta v^2}{4\pi G \mu}, \tag{3.1}$$

where G is the gravitational constant, $\mu = 4.58 \times 10^{-24}$ g is the gas mass per hydrogen molecule, and $\Delta v = \Delta v_5$ km s^{-1} is the Doppler parameter for the particles which dominate the hydrostatic support—in the case of molecular clouds, for H_2. The quantities κ and Δv are related to the core mass according to $M(<d) = 2\pi\kappa\mu d = \frac{1}{2}\Delta v^2 d/G$, where $M(<d)$ is the mass contained within a sphere of diameter d. For a cloud core of diameter 0.1 pc, the relationship is $M(<0.1\ \mathrm{pc}) = 11.6\Delta v_5^2\ M_\odot$.

With use of equation (3.1), we find that

$$\tilde{N}(\mathrm{HCl}) = \frac{x(\mathrm{HCl})\kappa r^{-1}}{\Delta v(\mathrm{HCl})} = \frac{\alpha x(\mathrm{HCl}) n(\mathrm{H_2})^{1/2}}{(4\pi G\mu)^{1/2}}, \tag{3.2}$$

where $\alpha \equiv \Delta v/\Delta v(\mathrm{HCl})$ is the ratio of velocity dispersion of the H_2 molecules to that of the HCl molecules. By a fortuitous cancellation (cf. NK93), the value of κ (or equivalently Δv) does not enter into the relationship between $\tilde{N}$(HCl) and $n(H_2)$. In high-mass cloud cores, where the line width is dominated by turbulent motions, the value of α is unity. In the inner regions of low-mass cloud cores, however, thermal motions may contribute significantly to the line width. In the limit where thermal motions dominate and turbulent motions are negligible, α is equal to $(m[\mathrm{HCl}]/m[\mathrm{H_2}])^{1/2} = 4.3$, where m[HCl] and $m[H_2]$ are the HCl and hydrogen molecular masses. While the results obtained below assume that turbulent motions dominate, i.e., that $\alpha = 1$, they may straightforwardly be rescaled to yield results for $\alpha \neq 1$, as described in Appendix B.

The total power radiated in line l is given by

$$P_l = \int 4\pi r^2 \Lambda_l\, dr = 2\pi\kappa^{3/2} \int \Lambda_l\, n(\mathrm{H_2})^{-5/2}\, dn(\mathrm{H_2}), \tag{3.3}$$

where Λ_l is the rate of emission per unit volume. Thanks to the simple relationship (eq. [3.1]) between $n(H_2)$ and $\tilde{N}$(HCl), Λ_l may be considered to be a function of $n(H_2)$, T, and x(HCl). Thus the quantity $P_l/\Delta v^3$ is a function of x(HCl) and T alone:

$$\frac{P_l}{\Delta v^3} = \frac{2\pi}{(4\pi G\mu)^{3/2}} \int \Lambda_l\, n(\mathrm{H_2})^{-5/2}\, dn(\mathrm{H_2}). \tag{3.4}$$

We have used the new collisional rate coefficients of Table 1 to compute Λ_l as a function of $n(H_2)$, adopting the standard escape probability method described by NK93. In determining the equilibrium level populations, we neglected the effects of radiative pumping. We then determined the integral in equation (3.4) between the limits $n(H_2) = 10^3$ cm^{-3} and $n(H_2) = 10^9$ cm^{-3}. Figure 1 shows the computed line luminosities as a function of x(HCl), for several temperatures. The upper panel shows the luminosity P_{10} of the $J = 1$–0 line (summed over the individual hyperfine components), the middle panel shows the luminosity P_{32} of the $J = 3$–2 line, and the lower panel shows the total luminosity in all rotational transitions, P_{tot}.

Due to the large quadrupole moment of the chlorine atom, the $J = 1$–0 line is split into three hyperfine components that were resolved by the observations of BKP. The frequency separation between these components being larger than the line-width in OMC-1, we have neglected line overlap effects. The predicted hyperfine line ratios are shown in Figure 2, where we have plotted the strengths of the $F = \frac{1}{2} \rightarrow \frac{1}{2}$ and $F = \frac{3}{2} \rightarrow \frac{1}{2}$ lines relative to that of the $F = \frac{5}{2} \rightarrow \frac{1}{2}$ line. In the limit of very low abundance, where optical depth effects are negligible, the line strengths lie in proportion to the statistical weights of the upper state, yielding a line ratio $\frac{1}{3}:\frac{1}{2}:1$. We note that the line strengths become more nearly equal as the abundance increases, but that a line ratio of 1:1:1 is never achieved. Thus the behavior in the limit of large abundance differs from the case of a uniform-density source, where the hyperfine components would attain equal strength once they all became effectively thick. In the isothermal sphere geometry considered here, the individual components do indeed become effectively thick but the size of the effectively thick emission region varies from one component to the next.

4. DISCUSSION

In the limit of very low HCl abundance, the $J = 1$–0 line luminosity at any given temperature shows a linear dependence upon x(HCl). In this regime, the line is optically thin at

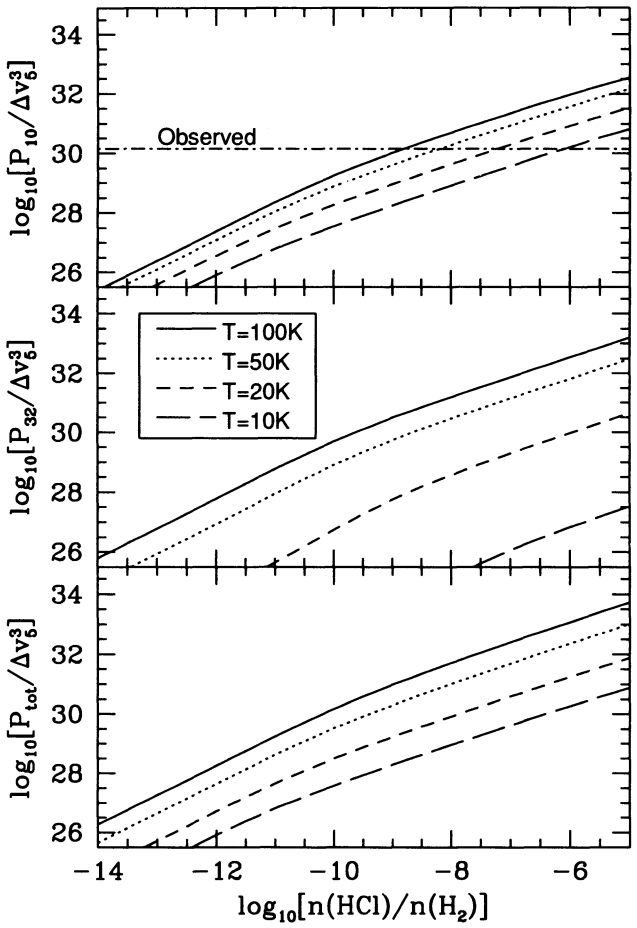

FIG. 1.—HCl line luminosities (ergs s^{-1}) as a function of HCl abundance, $x(\mathrm{HCl}) \equiv n(\mathrm{HCl})/n(\mathrm{H_2})$, for several temperatures (10, 20, 50, and 100 K). *Upper panel*: $J = 1$–0 line; *middle panel*: $J = 3$–2 line; *lower panel*: sum over all rotational lines. The dot-dashed line in the upper panel indicates the value observed by BKP.

all radii which contribute significantly to the integral in equation (3.3). At higher abundances, optical depth effects reduce the rate of increase of luminosity with abundance, and a $P_{10} \propto x(\mathrm{HCl})^{2/3}$ dependence ensues. An explanation of this behavior is provided by the approximate analytical treatment given in Appendix A.

As explained in Appendix A, the integral in equation (3.4) is dominated by emission close to the point at which the level populations thermalize. This fact is illustrated by Figure 3, which shows the power generated at densities $n(\mathrm{H_2}) > n$ as a function of n. We find that approximately one-half of the luminosity is generated within a range of densities covering only an order of magnitude. Thus the total power depends only weakly upon the upper and lower limits of our integration, provided that those limits bracket the density at which the contribution to the luminosity is maximal.

The $J = 1$–0 multiplet at 625.9 GHz has been detected by BKP toward OMC-1. Assuming that the source is much smaller than the 2′ diameter beam used in these observations, we may infer a line luminosity of 2.7×10^{31} ergs s^{-1}. The line width Δv appearing in equation (3.4) is most appropriately determined from the constant κ, with the use of equation (3.1). We follow BKP in fixing κ so as to match the total mass the source, inferred by Keene, Hildebrand, & Whitcomb (1982)

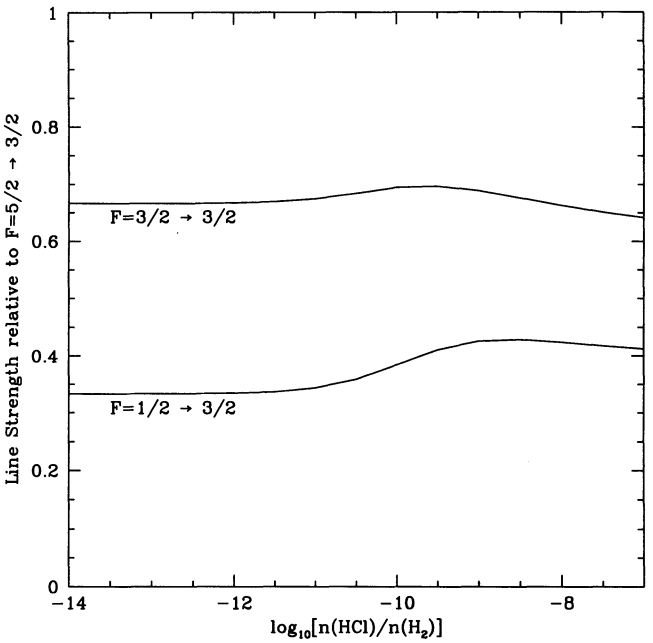

FIG. 2.—HCl $J = 1$–0 hyperfine line ratios as a function of HCl abundance, $x(\mathrm{HCl}) \equiv n(\mathrm{HCl})/n(\mathrm{H_2})$. Results apply to the ratios $P(F = \frac{3}{2} \rightarrow \frac{1}{2})/P(F = \frac{5}{2} \rightarrow \frac{1}{2})$ (*upper curve*) and $P(F = \frac{1}{2} \rightarrow \frac{1}{2})/P(F = \frac{5}{2} \rightarrow \frac{1}{2})$ (*lower curve*).

from 400 μm continuum measurements to be 50 $M_\odot$ within the central 35″. This constraint yields a line width $\Delta v_5 = 2.3$—corresponding to a FWHM of 4.2 km s^{-1}—in good agreement with the observed widths of HCl $J = 1$–0 and other high-density tracers. These observational parameters therefore indicate a value of 1.8×10^{30} ergs s^{-1} for $P_{10}/\Delta v_5^3$. The temperature of the dense quiescent gas in Orion-KL varies with location over the range 70–200 K (Genzel & Stutzki 1989).

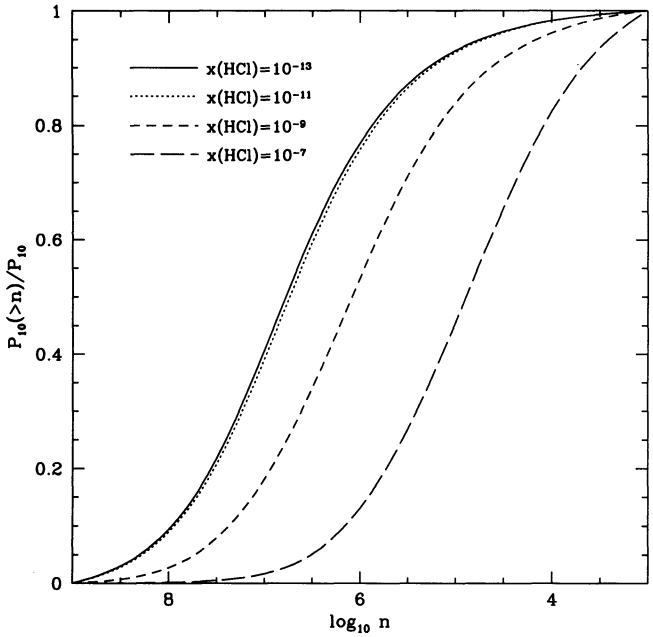

FIG. 3.—Fraction of HCl $J = 1$–0 luminosity generated at H_2 particle densities greater than n within a singular isothermal sphere. Results apply to $T = 100$ K, and are shown for abundances $x(\mathrm{HCl}) = 10^{-13}$ (*leftmost curve*), 10^{-11}, 10^{-9}, and 10^{-7} (*rightmost curve*).

Taking 100 K as a typical value for the gas temperature, the results plotted in Figure 1 show that an abundance $x(\mathrm{HCl}) = 2 \times 10^{-9}$ may be inferred. In the absence of reliable error estimates for such parameters as the line luminosity, the line width, or the core mass in OMC-1, we are unable to derive meaningful error estimates for our derived abundance. We do note, however, that the derived abundance depends quite strongly on some of the observational parameters, viz., $x(\mathrm{HCl}) \propto P_{10}^{3/2}$, $x(\mathrm{HCl}) \propto \Delta v^{-9/2}$, $x(\mathrm{HCl}) \propto [M(<0.1\ \mathrm{pc})]^{-9/4}$, and $x(\mathrm{HCl}) \propto T^{-1.7}$. These relatively strong dependences imply that the true HCl abundance might differ significantly from our "best estimate" of 2×10^{-9}.

The peak antenna temperatures measured by BKP for the individual hyperfine components lie in the ratio 0.3:0.8:1, in reasonable agreement with the ratio of 0.43:0.68:1 predicted for $x(\mathrm{HCl}) = 2 \times 10^{-9}$ (Fig. 2). Following the discussion in § 3 above, however, we note that the observed hyperfine ratio (although it differs significantly from 1:1:1) does not place *any* meaningful upper limit on the HCl abundance nor upon the line optical depths in the central part of the source.

Unless chlorine is highly depleted onto interstellar dust grains within dense molecular clouds, our estimate of the HCl abundance suggests that only a small fraction of the gas-phase chlorine nuclei are to be found in HCl, contrary to theoretical expectations (Dalgarno et al. 1974; Adams & Smith 1985; Blake, Anicich, & Huntress 1986). We note, however, that theoretical models for the chemistry of chlorine-bearing species in dense molecular clouds have thus far neglected the photodissociation of HCl by ultraviolet photons in the H_2 Lyman and Werner bands: such photons are generated within dense clouds following the excitation of H_2 by the fast secondary electrons that result from cosmic-ray ionization (Prasad & Tarafdar 1983) and are predicted to affect significantly the abundance of several species (Sternberg, Lepp, & Dalgarno 1987). We speculate that cosmic-ray induced photodissociation may be a significant destruction mechanism for HCl, and that its neglect may lead to predictions for the abundance of HCl that are too large. Detailed chemical models will be needed to address this speculation.

HCl is not expected to be a major coolant of dense cloud cores. Figure 1 indicates that for $x(\mathrm{HCl}) \geq 10^{-10}$ and $10\ \mathrm{K} \leq T \leq 100\ \mathrm{K}$ the total luminosity carried in HCl lines is given by

$$\frac{P_{\mathrm{tot}}(\mathrm{HCl})}{\Delta v_5^3} \sim 1.0 \times 10^{31} \left(\frac{T}{100\ \mathrm{K}}\right)^{2.8} \left[\frac{x(\mathrm{HCl})}{10^{-9}}\right]^{2/3} \mathrm{ergs\ s^{-1}}. \quad (4.1)$$

If the HCl abundance is only 2×10^{-9}, HCl transitions do not make a significant contribution to the total molecular line luminosity. Analogous calculations for water (Neufeld 1993), which make use of the rate constants of Green, Maluendes, & Mclean (1993), indicate a corresponding water line luminosity of

$$\frac{P_{\mathrm{tot}}(\mathrm{H_2O})}{\Delta v_5^3} \sim 0.8 \times 10^{31} \left(\frac{T}{100\ \mathrm{K}}\right)^{3.0} \left[\frac{x(\mathrm{H_2O})}{10^{-9}}\right]^{2/3} \mathrm{ergs\ s^{-1}}. \quad (4.2)$$

The water abundance in dense molecular cloud cores has yet to be measured reliably, but models for interstellar chemistry predict $x(\mathrm{H_2O}) \equiv n(\mathrm{H_2O})/n(\mathrm{H_2}) \sim 10^{-6}$. If that prediction proves correct, then $P_{\mathrm{tot}}(\mathrm{HCl})/P_{\mathrm{tot}}(\mathrm{H_2O})$ is only ~ 0.02. Our estimate of the HCl abundance suggests that HCl is probably comparable *not to* $H_2^{16}O$ *but rather to the isotopically substituted* $H_2^{18}O$ *molecule*, both in its abundance and in its contribution to the total cooling. Furthermore, the $J = 1$–0 HCl transition is quite closely analogous to the 1_{10}–1_{01} transition of $H_2^{18}O$ near 547.7 GHz. At a temperature of 100 K, the predicted line luminosities are $1.03 \times 10^{30} \Delta v_5^3 [x(\mathrm{HCl})/10^{-9}]^{2/3}$ and $0.24 \times 10^{30} \Delta v_5^3 [x(\mathrm{H_2O})/10^{-9}]^{2/3}$ ergs s^{-1}, respectively. Observations of the 547.7 GHz transition of $H_2^{18}O$ and of the analogous transition of $H_2^{16}O$ near 556.9 GHz will be carried out using the *Submillimeter Wave Astronomy Satellite*; models such as that developed here for the excitation of HCl will then allow the water abundance to be determined in dense molecular cloud cores.

Figure 1 indicates that at a temperature of 100 K, the $J = 1$–0 line accounts for less than 10% of the total HCl luminosity. Most of the HCl emission emerges in higher lying transitions, such as the $J = 3$–2 line near 159.8 μm. Unlike the $J = 2$–1 line, the $J = 3$–2 transition has a short enough wavelength to be potentially detectable using photoconductive detectors. The results for P_{32} plotted in Figure 1 indicate that a $J = 3$–2 flux of $\sim 10^{-19}$ W cm^{-2} is expected from OMC-1, suggesting that the Long-Wavelength Spectrometer of the *Infrared Space Observatory* could be used to measure the line strength. Such a measurement would provide a useful test of our model for the excitation of HCl in OMC-1. In addition, as suggested by BKP, observations of $J = 1$–0 emission from the less abundant $H^{37}Cl$ isotope would serve as a further probe of the HCl abundance. Given an abundance ratio $H^{35}Cl/H^{37}Cl = 3.1$, our model makes the specific prediction that the strength of the $H^{37}Cl$ $J = 1$–0 line near 625.0 GHz will lie a factor $3.1^{2/3} = 2.1$ below that observed for the $H^{35}Cl$ $J = 1$–0 line. The hyperfine line ratios are predicted to be nearly the same for the two isotopes.

5. SUMMARY

We have computed new rate coefficients for the collisional excitation of HCl by He, in the close-coupling formalism and with the use of the DCl–He interaction potential determined by Willey et al. (1992). Results have been obtained for temperatures between 10 K and 300 K. We have also calculated pressure-broadening cross sections and found them to be in good agreement with the experimental values measured by Giraud et al. (1970). With the use of the infinite order sudden approximation, we have derived approximate expressions of general applicability which may be used to estimate how the rate constant for a transition $(J \rightarrow J')$ is apportioned among the various hyperfine states F' of the final state J'.

Approximating a dense molecular core as a singular isothermal sphere, and using an escape probability method to solve for the HCl rotational level populations, we obtained predictions for the HCl rotational line strengths as a function of the HCl abundance. Over a wide range of HCl abundances, we have found that the line luminosities are proportional to (abundance)$^{2/3}$, a result which can be explained using a simple analytical approximation. This is a result of general applicability which may prove useful in interpreting observations of other hydrides, such as those planned for the species H_2O and $H_2^{18}O$ using the *Submillimeter Wave Astronomy Satelite.*

Using our results to reinterpret the $H^{35}Cl$ $J = 1$–0 observations of BKP toward the source OMC-1, we derived an abundance $n(\mathrm{HCl})/n(\mathrm{H_2}) = 2 \times 10^{-9}$, which amounts to $\sim 0.3\%$ of the total Cl elemental abundance. Unless chlorine is highly depleted onto interstellar dust grains within dense molecular clouds, our estimate of the HCl abundance suggests that only a

small fraction of the gas-phase chlorine nuclei are to be found in HCl. We speculate that the effects of cosmic-ray induced photodissociation may explain why the HCl abundance is apparently smaller than the predictions of previous models for the chemistry of chlorine-bearing species in dense molecular clouds. Our predictions for the hyperfine line ratios within the $J = 1$–0 multiplet are in reasonable agreement with the observed values; in contrast to what would be expected for a uniformly dense cloud, our model for the singular isothermal sphere predicts hyperfine line ratios significantly different from 1:1:1—as indeed is observed—even if the lines are highly optically thick at the center of the cloud core. Our estimate of the HCl abundance implies that HCl transitions do not carry a significant fraction of the power radiated by molecular emissions from dense molecular cloud cores: based on current chemical models, we expect the power radiated by H_2O transitions to exceed that radiated by HCl by approximately two orders of magnitude.

Our model for the excitation of HCl in dense molecular cloud cores makes specific, testable predictions for the strengths of transitions which have yet to be observed. We find (1) that the $J = 1$–0 transition of $H^{37}Cl$ near 625.0 GHz is expected to be less luminous than the analogous $H^{35}Cl$ transition by a factor of 2.1; and (2) that the $J = 3$–2 transition of $H^{35}Cl$ near 159.8 μm is expected to show a line flux toward OMC-1 of $\sim 10^{-19}$ W cm^{-2}, suggesting that it can be detected using the *Infrared Space Observatory*.

Note added in *manuscript*.—Zmuidzinas and collaborators have recently detected the $J = 1$–0 line of $H^{35}Cl$ in absorption toward Sgr B2 (J. Zmuidzinas, private communication). They estimate the abundance x(HCl) as $\sim 1 \times 10^{-9}$, assuming a molecular hydrogen column density of 2×10^{23} cm^{-2} in the absorbing envelope. This value is to be regarded as a lower limit, because they assumed that all molecules are in the ground state and that the dust continuum source is entirely behind the absorbing cloud. Although the Sgr B2 observation probes the HCl abundance in a region which is potentially quite different from OMC-1, the abundance derived by Zmuidzias and collaborators lies close to the value obtained in our analysis of the HCl emission from OMC-1: it supports the notion that HCl accounts for only a small fraction of the elemental chlorine within the dense interstellar medium.

D. A. N. gratefully acknowledges the support of NASA grant NAGW-3147 from the Long-Term Space Astrophysics Research Program. S. G. was supported in part by NASA Headquarters, Office of Space Sciences and Applications, Astrophysics Division, Infrared and Radio Astrophysics Program.

APPENDIX A

APPROXIMATE ANALYTICAL TREATMENT

We may obtain an approximate analytic expression for the power radiated in the $J = 1$–0 line. In the low-density limit, most molecules lie in the $J = 0$ state, and the rate of emission per unit volume from hyperfine state i of the $J = 1$ state is

$$\Lambda_i = x(\mathrm{HCl}) n(\mathrm{H_2})^2 \gamma_{0i} \Delta E \,, \tag{A1}$$

where γ_{0i} is the rate coefficient for collisional excitation from the ground state to state i and ΔE is the transition energy. Above the density required for thermalization, $n_{\mathrm{th},i}$, the emission rate Λ_i increases less rapidly with density. In the optically thin limit, $\Lambda_i \propto n(\mathrm{H_2})$, while in the optically thick limit $\Lambda_i \propto n(\mathrm{H_2}) \tilde{N}(\mathrm{HCl})^{-1} \propto n(\mathrm{H_2})^{1/2}$. In either case, the high-density behavior guarantees the integral for the total power

$$P_i = \int 4\pi r^2 \Lambda_i \, dr = 2\pi \kappa^{3/2} \int \Lambda_i \, n(\mathrm{H_2})^{-5/2} \, dn(\mathrm{H_2}) \tag{A2}$$

(eq. [3.3]) converges at large $n(\mathrm{H_2})$, while the low-density behavior implies that the integral converges at small $n(\mathrm{H_2})$. The maximum contribution to the integral occurs near $n(\mathrm{H_2}) = n_{\mathrm{th},i}$. To within a factor of order unity, we may estimate the total power as

$$P_i \sim 2\pi \kappa^{3/2} x(\mathrm{HCl}) n_{\mathrm{th},i}^{1/2} \gamma_{0i} \Delta E \,. \tag{A3}$$

If the HCl abundance is very small, the $J = 1$–0 line remains optically thin up to and beyond the density at which the upper state thermalizes. The density for thermalization is then equal to the critical density, $n_{\mathrm{cr},i} \equiv A/\gamma_{i0}$, and our estimate for the total power becomes

$$P_i(\mathrm{thin}) \sim 2\pi \kappa^{3/2} x(\mathrm{HCl}) (A/\gamma_{i0})^{1/2} \gamma_{0i} \Delta E \,. \tag{A4}$$

With the help of equation (3.1), we may rewrite this result in the form

$$\frac{P_i(\mathrm{thin})}{\Delta E \, \Delta v^3} \sim \frac{2\pi}{(4\pi G \mu)^{3/2}} \, x(\mathrm{HCl}) (A \gamma_{i0})^{1/2} \left(\frac{g_i}{g_0} \right) \exp\left(-\frac{\Delta E}{kT} \right), \tag{A5}$$

where $g_i = 2F + 1$ are the degeneracies of the $J = 1$ states and where $g_0 = 4$ is the degeneracy of the ground state. In the low-abundance limit, the total power increases in proportion to the HCl abundance. The hyperfine line strengths are predicted to lie in the ratio of the g_i, i.e., in the ratio $\frac{1}{3}:\frac{1}{2}:1$.

As the HCl abundance increases, the $J = 1$–0 transitions eventually become optically thick at a density smaller than n_{cr}. In this regime, the thermalization density is smaller than the critical density by a factor of order the line optical depth. When most molecules lie in the ground state, the line optical depths are given by

$$\tau = \frac{(g_i/g_0)A\tilde{N}(\mathrm{HCl})}{8\pi\sigma^3}, \tag{A6}$$

where σ is the transition wavenumber. The thermalization density may then be estimated using the expression

$$\frac{n_{cr}}{n_{th,i}} \sim \frac{(g_0/g_i)A\tilde{N}(\mathrm{HCl})}{8\pi\sigma^3} = \frac{(g_0/g_i)Ax(\mathrm{HCl})n_{th,i}^{1/2}\alpha}{(4\pi G\mu)^{1/2}(8\pi\sigma^3)}, \tag{A7}$$

which yields the solution

$$n_{th,i} \sim \left[\frac{(4\pi G\mu)^{1/2}(8\pi\sigma^3)(g_0/g_i)}{x\gamma_{i0}\alpha}\right]^{2/3}. \tag{A8}$$

Substituting into equation (A3), we may estimate the total power as

$$\frac{P_i(\mathrm{thick})}{\Delta E\,\Delta v^3} \sim \frac{2\pi}{(4\pi G\mu)^{4/3}} x(\mathrm{HCl})^{2/3}(2\pi^{1/3}\sigma)\gamma_{i0}^{2/3}\left(\frac{g_i}{g_0}\right)^{2/3}\alpha^{-1/3}\exp\left(-\frac{\Delta E}{kT}\right). \tag{A9}$$

If the HCl abundance is sufficient to make the transitions optically thick at a density smaller than n_{cr}, the total power $P_i \propto x(\mathrm{HCl})^{2/3}$. This is precisely the behavior exhibited by the results plotted in Figure 1. The hyperfine line strengths are predicted by our approximate analytical treatment to lie in the ratio of the $g_i^{2/3}$, i.e., in the ratio 0.45:0.76:1, in fairly good agreement with the exact results plotted in Figure 3.

APPENDIX B

SCALING RELATIONS

The results presented in Figure 1 are based upon the assumption that the ratio α of the H_2 Doppler parameter to the HCl Doppler parameter is unity. Thus if $\alpha \neq 1$, the relationship between $\tilde{N}$ and $n(H_2)$ (eq. [3.2]) is different from what we assumed in our calculation. A simple scaling of the HCl abundance allows the appropriate correction to be made: the radiated power for the $\alpha \neq 1$ case is

$$\mathrm{Power} = \alpha P[\alpha^{-1}x(\mathrm{HCl})], \tag{B1}$$

where P is the power plotted in Figure 1 for $\alpha = 1$. In the limit of very small abundance, where $P \propto x(\mathrm{HCl})$, equation (B1) implies that the line luminosities are independent of α, as expected because optical depth effects are negligible. In the regime of larger abundance, where $P \propto x(\mathrm{HCl})^{2/3}$, the luminosity is proportional to $\alpha^{-1/3}$ (see also Appendix A). In a static cloud core, the value of α can vary only between 1 (pure turbulence) and 4.3 (purely thermal line width), so the quantity $\alpha^{-1/3}$ varies only over the range 0.62–1.0.

Another scaling allows our results to be applied to the case of a constant velocity outflow, for which a $n(H_2) = \kappa r^{-2}$ dependence would also obtain. In such an outflow, the constant κ is given by

$$\kappa = \frac{\dot{M}}{4\pi v_r \mu}, \tag{B2}$$

where $\dot{M}$ is the mass outflow rate and v_r is the outflow velocity. Comparing this result with the expression for κ in the static case (eq. [3.1]), we find that the results obtained in § 3 and § 4 may be applied to the constant velocity outflow if $(G\dot{M}/v_r)^{1/2}$ is everywhere substituted in place of Δv. In a *supersonic* constant velocity outflow, the optical depth parameter is given by

$$\tilde{N} = \frac{x(\mathrm{HCl})n(H_2)r}{2v_r} \tag{B3}$$

(Neufeld & Kaufman 1993). Comparing this expression with equation (3.2), we find that the appropriate value of the dimensionless factor α is

$$\alpha = \frac{1}{2}\left(\frac{G\dot{M}}{v_r^3}\right)^{1/2}. \tag{B4a}$$

If the outflow is subsonic, $\tilde{N} = x(\mathrm{HCl})\kappa r^{-1}/\Delta v(\mathrm{HCl})$—as in the static case—and

$$\alpha = \frac{1}{\Delta v(\mathrm{HCl})}\left(\frac{G\dot{M}}{v_r}\right)^{1/2}. \tag{B4b}$$

Thus the static core results that were obtained in this paper may be applied to the case of a constant velocity outflow with the use of the scaling (B1)—and the expressions for α given by equations (B4a) or (B4b)—along with the substitution of $(G\dot{M}/v_r)^{1/2}$ for every occurrence of Δv.

REFERENCES

Adams, N. G., & Smith, D. 1985, ApJ, 298, 827
Alexander, M. H., & Manolopoulos, D. E. 1987, J. Chem. Phys., 86, 2044
Blake, G. A., Anicich, V. G., & Huntress, W. T., Jr. 1986, ApJ, 300, 415
Blake, G. A., Keene, J., & Phillips, T. G. 1985, ApJ, 295, 501 (BKP)
Collins, L. A., & Lane, N. F. 1975, Phys. Rev. A., 12, 811
Corey, G. C., & McCourt, F. R. 1983, J. Phys. Chem., 87, 2737
Dalgarno, A., de Jong, T., Oppenheimer, M., & Black, J. H. 1974, ApJ, 192, L37
Fuller, G. A., & Myers, P. C. 1993, ApJ, 418, 273
Genzel, R., & Stutzki, J. 1989, ARA&A, 27, 41
Giraud, M., Robert, D., & Galatry, L. 1979, J. Chem. Phys., 52, 312
Goldsmith, P. F., & Langer, W. D. 1978, ApJ, 222, 881
Goldsmith, P. F., Lamger, W. D., Schloerb, F. P., & Scoville, N. Z. 1980, ApJ, 240, 524
Goodman, A. A., Benson, P. J., Fuller, G. A., & Myers, P. C. 1993, ApJ, 406, 528
Green, S. 1977a, J. Chem. Phys., 67, 715
———. 1977b, Chem. Phys. Lett., 47, 119
———. 1988, J. Chem. Phys., 88, 7331
Green, S., & Monchick, L. 1975, J. Chem. Phys., 63, 4198
Green, S., Maluendes, S., & McLean, A. D. 1993, ApJS, 85, 181
Held, W. D., Piper, E., Ringer, G., & Toennies, J. P. 1980, Chem. Phys. Lett., 75, 260
Keene, J., Hildebrand, R. H., & Whitcomb, S. E. 1982, ApJ, 252, L11
Keto, E. R., Ho, P. T. P., & Haschick, A. D. 1988, ApJ, 324, 920
Larson, R. B. 1969, MNRAS, 145, 271
Lovejoy, C. M., & Nesbitt, D. 1990, J. Chem. Phys., 93, 5387
Monteiro, T. S., & Stutzki, J. 1986, MNRAS, 221, 33P
Myers, P. C., & Caselli, P. 1993, private communication
Myers, P. C., & Fuller, G. A. 1992, ApJ, 396, 631
Neufeld, D. A. 1993, SWAS Tech. Memor. 8007A, issued by the *Submillimeter Wave Astronomy Satellite* Program
Neufeld, D. A., & Kaufman, M. J. 1993, ApJ, 418, 263 (NK93)
Neufeld, D. A., Lepp, S., & Melnick, G. J. 1994, in preparation
Prasad, S. S., & Tarafdar, S. P. 1983, ApJ, 267, 603
Sternberg, A., Lepp, S., & Dalgarno, A. 1987, ApJ, 320, 676
Varshalovich, D. A., & Khersonsky, V. K. 1977, Astrophys. Lett., 18, 167
Willey, D. R., Choong, V.-E., & DeLucia, F. C. 1992, J. Chem. Phys., 96, 898